ADVANCED OPTICAL MATERIALS
www.advopticalmat.de

Ultrafast Multistage Lattice Strain via Laser-Excited Phonons in Lithium Niobate

Bo Wu, Qing Yang, Bin Zhang, Lei Wang, Yingying Ren, Sheng Meng, and Feng Chen**

Ultrafast laser-excitation of lithium niobate ($LiNbO_3$) crystal has triggered numerous photonic applications through the structural transitions in $LiNbO_3$. However, the explanations for ultrafast laser-induced modification of $LiNbO_3$ have remained phenomenological, lacking a convincing in-depth understanding of the fundamental laser-lattice interaction process. Based on ab initio simulations, it is demonstrated that photoexcited anharmonic phonons play a significant role in influencing the lattice structure of $LiNbO_3$. Harnessing the real-time time-dependent density functional theory, it is revealed that the excitation of TO_4 phonons via electric-phonon coupling triggers displacement-induced lattice oscillations during multiphoton ionization. These oscillations give rise to multistage structural strains, resulting in alterations of the refractive index. Significantly, these modifications exhibit sensitivity to the incident laser energy. Experimentally, using the waveguide technique and micro-Raman spectroscopy, the correlation between local refractive index, lattice volume density, and phonon vibrational modes has been established, exhibiting good consistency with theoretical predictions. This work provides an effective means to understand the ultrafast excitation of phonons and relaxation processes of the lattice in dielectric crystals.

1. Introduction

The exquisite manipulation of electronic and structural properties through ultrafast laser-matter interactions has become a prominent subject in the field of ultrafast science due to its rich physical phenomena and fascinating applications across multiple domains.[1–4] In the ultrashort timescales, a variety of complex processes emerge, for example, the non-thermal fusion of amorphous states, lattice densification, and Coulomb micro-explosion due to nonlinear processes (multiphoton absorption, tunnel ionization, and avalanche ionization).[5–8] Thus, comprehending the fundamental physical mechanisms and dynamic evolution of laser-matter interactions is essential for the precise control of materials' properties.

$LiNbO_3$ crystal, also known as the "*Silicon of Photonics*," boasts exceptional properties that make it a versatile platform for a myriad of applications.[9] Ultrafast laser processing has become an essential tool in $LiNbO_3$ photonics, enabling the production of high-quality micro-disk resonators, three-dimensional (3D) waveguide devices, and self-organized nanogratings.[4,10–13] Recent studies have also shown that ultrafast laser pulses can selectively reverse the polarization of $LiNbO_3$ ferroelectric domains, enabling the development of 3D nonlinear photonic crystals.[14–17] Despite these advances in applications, the explanations for various complex phenomena remain at a relatively macroscopic level.[18–20] The specific driving mechanisms behind the laser-induced lattice strains and resulting displacive-type structural transitions are still unclear, and the connection between microscopic motion and macroscopic evolution has not been established.[14,21,22] Therefore, to precisely tailor $LiNbO_3$, it is imperative to gain a comprehensive understanding of the fundamental mechanisms and dynamic evolution of laser-lattice interaction.

Significant progress has been achieved in comprehending the theoretical underpinnings and experimental observations of laser-induced phase transitions in diverse materials.[23–25] Notably, utilizing ultrafast time-resolved X-ray diffraction techniques, researchers have uncovered that laser irradiation causes perturbations in resonant bonds of 2D semiconductor materials, leading to local structural distortions and non-thermal lattice expansion.[26–29] However, the $LiNbO_3$ crystal presents a significant challenge due to the intricate nature of its excited-state

B. Wu, B. Zhang, L. Wang, F. Chen
School of Physics
State Key Laboratory of Crystal Materials
Shandong University
Jinan 250100, China
E-mail: drfchen@sdu.edu.cn
Q. Yang, S. Meng
Beijing National Laboratory for Condensed Matter Physics and Institute of Physics
Chinese Academy of Sciences
Beijing 100190, China
E-mail: smeng@iphy.ac.cn
Y. Ren
Shandong Provincial Engineering and Technical Center of Light Manipulations and Shandong Provincial Key Laboratory of Optics and Photonic Device
School of Physics and Electronics
Shandong Normal University
Jinan 250358, China

The ORCID identification number(s) for the author(s) of this article can be found under https://doi.org/10.1002/adom.202302106

DOI: 10.1002/adom.202302106

resonant bonds and phonon spectra, which are usually accompanied by intense nonlinear signal radiation.[30] Although second harmonic phase-sensitive measurements and transient detection of specific phonon amplitude changes have been achieved experimentally,[14,31,32] these techniques are insufficient to investigate the mesoscopic transient dynamics of the lattice, such as the lattice deformation.

The theoretical models based on density functional theory (DFT) have been employed to elucidate the phonon-lattice dynamics that occur in laser-induced dielectrics.[33,34] During the process of electron-phonon coupling, the stimulated vibrations of phonons play a crucial role in atomic motion and the generation of non-thermal modulations in the lattice.[35,36] However, the complex multistage physical processes of $LiNbO_3$ require theoretical models with increased degrees of freedom and precision to accurately describe its structural properties.[37] To address this, time-dependent ab initio simulation based on real-time time-dependent density functional theory (rt-TDDFT) with momentum resolution has been employed to demonstrate the evolution behavior of electrons and atoms.[38,39] This technique has been successfully applied in laser-induced phase-change materials.[40] By simplifying the real-time evolution of the wave function of multi-electron systems under externally applied optical fields, the rt-TDDFT simulation provides access to the system's absorption spectrum and the dynamics of excited states, enabling the 3D modeling of complex $LiNbO_3$ lattice systems.

In this letter, we explore the intricate electron-lattice coupling dynamics of the $LiNbO_3$ lattice using the rt-TDDFT simulation. The electron–phonon coupling effect induces an ordered modulation on the anisotropic lattice, resulting in the activation of the anharmonic phonon mode (A_1-TO_4), which is present as the active vibrational mode in Raman spectra.[14,30] The displacement excitation of this mode leads to oriented forces (stress) in the oxygen octahedra (NbO_6), forcing oriented lattice strain. We observe the transient dynamic evolutions of lattice-induced lattice contraction/expansion under varying excitation levels in less than 1 ps. Experimentally, we achieve modulation of the lattice refractive index from positive to negative through the femtosecond laser processing. The analysis is performed using waveguide and micro-Raman scattering techniques, yielding results consistent with calculations. This ordered manipulation of the $LiNbO_3$ volume offers the ability to tailor the local refractive index on-demand, forming waveguide structures for photonic applications.[41,42]

2. Results

2.1. Laser-$LiNbO_3$ Interaction

$LiNbO_3$ belongs to the trigonal crystalline system, which contains a symmetrical triple *c*-axis and an ABO_3-type crystal structure.[33] The atoms are stacked as AB–AB stacking, forming an oxygen octahedral void structure (NbO_6) with anisotropic structural features (**Figure 1**a). The ultrafast laser-induced modifications in $LiNbO_3$ are mainly caused by nonlinear absorption,[14,36] which promotes the valence electrons to the conduction band, mainly through multiphoton and avalanche ionizations (Figure 1b). As the energy of stimulated carriers (electron–phonon coupling) is gradually transferred to the entire lattice, femtosecond laser pulses generate strong non-equilibrium conditions in materials. In the sub-picosecond timescale, the electron temperature is much higher than the lattice temperature, in which the phonons dominate the lattice modulation.[29]

2.1.1. Displacement Excitation of Phonons in Interaction with Ultrafast Light Fields

We utilize the rt-TDDFT (Notes S1–S3, Supporting Information) to simulate the transient dynamic evolution of the $LiNbO_3$ model. During this process, the excitation of specific phonon vibrational modes plays a crucial role in inducing phase transitions.[35,36] The time evolution of each phonon branch is explored by projecting the displacement of ions in the trajectory onto the phonon eigenvectors calculated from the equilibrium ground state. The projection intensity is defined as $\sum e_i \cdot u_j$, where u_j is the displacement vector of atom j from its original position at $t = 0$, and e_i is the ith phonon eigenvector at the Γ point (Notes S2, Supporting Information). As ultrafast laser irradiates the lattice, the coupling strength between the lattice and charge carriers increases during the energy relaxation process, resulting in the excitation of specific phonon modes (oxygen octahedron vibration, A_1-TO_4, Figure S1, Supporting Information). Additionally, we observe an alternative excitation mode for the "soft mode" A_1-TO_1 (Figure S2, Supporting Information). This soft mode mainly influences the ferroelectric polarization of the lattice while having a lesser impact on its lattice strain. Therefore, the TO_4 mode is an effective tool for studying phonon-lattice coupling in $LiNbO_3$. From Figure 1c, it is found that with high laser energy (0.0453 mJ cm^{-2}), the non-equilibrium position vibration of the TO_4 mode approximates simple harmonic motion. This indicates that phonons are excited at relatively stable positions, resulting in the emergence of new modes and representing the occurrence of lattice phase transition. This vibrational mode signifies the stretching of individual oxygen octahedra (Figure 1d), leading to an increase in the Nb–O_1 bond length and a decrease in the Nb–O_2 bond length, which affects the lattice volume structure. Additionally, in contrast to the fast decay of typical coherent phonons oscillations, the oscillations of the TO_4 mode at non-equilibrium positions remain metastable. This observation suggests that the stress between its constituent atoms persists and exerts a more substantial impact on the lattice strain.

2.1.2. Ultrafast Multistage Dynamic Lattice Evolution

Moreover, the dynamic evolution trend of the lattice depends on the projection direction of the characteristic vector of phonons relative to the axial direction. This leads to significant directional dependence in the laser-induced lattice strains in anisotropic $LiNbO_3$ structure. We use the laser fields with low energies (0.0163 and 0.0290 mJ cm^{-2}) and high energies (0.0453 and 0.0548 mJ cm^{-2}) to simulate the lattice. Under the irradiation of different energies, the lattice structure exhibits significant directional differences in its evolution. Under weak laser excitation, the lattice along the *c*-axis generates oscillation below the equilibrium position, which shows a slight contraction strain (**Figure 2**a). Predictably, the lattice along the *a*-axis displays os-

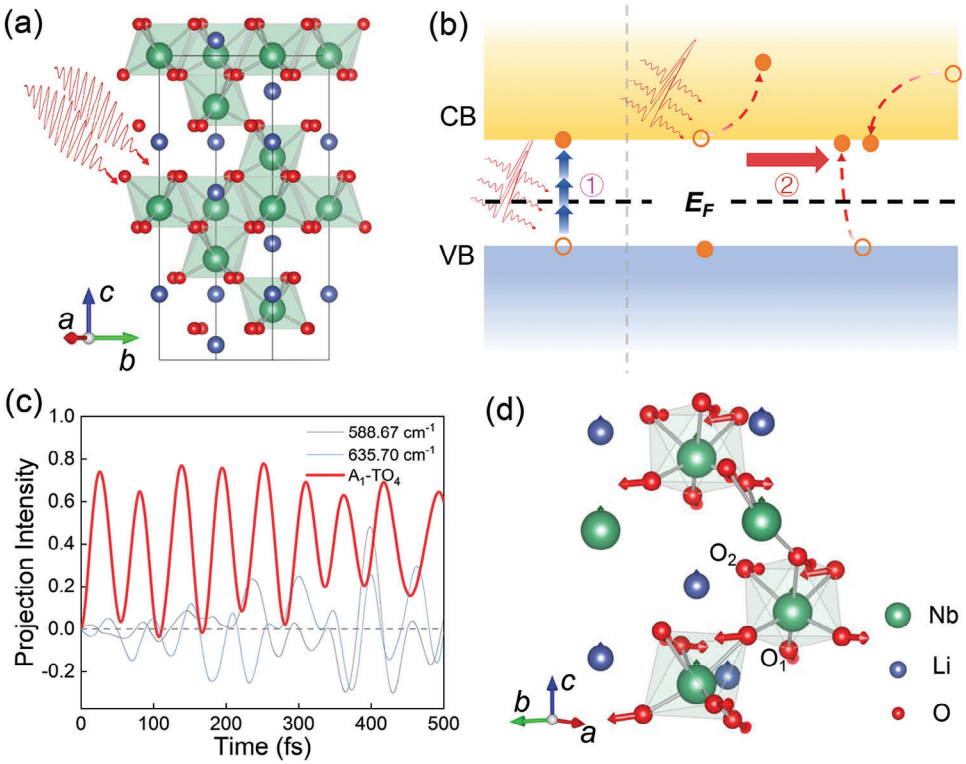

Figure 1. a) $LiNbO_3$ lattice in side view. b) Nonlinear photoionization processes underlying laser irradiation: multiphoton ionization (1) and avalanche ionization (2). c) Time evolution of displacement excitation of specific phonon mode (A_1-TO_4, the Γ point at 620.11 cm^{-1}) under a strong laser field. Other adjacent phonons (black and blue lines, at 588.67 and 635.70 cm^{-1}) oscillate at the equilibrium position. d) Schematics of the motions associated with the TO_4 mode. Nb and Li move along +*c*-axis, and the component of O atoms along *c*-axis direction is always downward.

cillation near the equilibrium position and indicates a tendency for the lattice to expand slightly (Figure 2b).

However, as the intensity of the laser reaches a sufficient level, the coupling between the lattice and charge carriers is strengthened during the energy relaxation process, which has the potential to drive the system far away from its equilibrium positions. This is illustrated in Figure 2c, which shows that under high-fluence laser irradiation, the lattice strain process can be divided into three stages along the *c*-axis. In the initial stage (Stage 1), the electron-phonon coupling plays a dominant role, and the phonon energy has not yet been transferred to the lattice. At this stage, the lattice oscillates based on its equilibrium positions. In Stage 2, the energy gradually transfers from phonons to the lattice, and the modulating influence of TO_4 mode on the lattice becomes increasingly evident. Under the influence of "internal" stress, the lattice undergoes a rapid contraction at around 500 fs, reaching its maximum at around 800 fs. Due to the orderliness and stability of the $LiNbO_3$ lattice, the lattice rapidly rebounds and exhibits an expansion strain (Stage 3) as the internal rebound stress exceeds the compressive stress generated by phonon-lattice coupling. The lattice deformation accelerates with increasing energy. Furthermore, the lattice along the *a*-axis consistently exhibits an expansion effect, and as the energy increases, the lattice expands faster (Figure 2d). With increasing energy, the lattice expansion significantly accelerates. When the expansion rate exceeds 25%, the entire lattice is observed to have been completely fractured, exhibiting a disordered atomic arrangement and categorizing it as being damaged (see Figure S3, Supporting Information).It is worth noting that the lattice damage threshold in the experiment is higher than that in the simulation due to the systematical error from the simulation (such as uniform excitation and periodic boundary conditions), which causes an overestimation of lattice changes.

2.2. Refractive Index as a Function of Lattice Strain

The refractive index is an intuitive physical parameter that is sensitive the volume changes. Based on DFT, we calculate the lattice volume changes under different oriented stresses in $LiNbO_3$. The numerical relationship between lattice strain, dielectric constant, and refractive index is elucidated and the axial lattice variation is linked to the refractive index variation (Note S5, Supporting Information),

$$n(\omega) = \left[\frac{\sqrt{\epsilon_1^2(\omega) + \epsilon_2^2(\omega)} + \epsilon_1(\omega)}{2}\right]^{\frac{1}{2}} \quad (1)$$

where $\epsilon_1(\omega)$ and $\epsilon_2(\omega)$ are the real and imaginary parts of the dielectric function, and ω is the photon frequency. As shown in **Figure 3**, the structural changes of the lattice under stress and the corresponding refractive index difference (Δn) exhibit an approx-

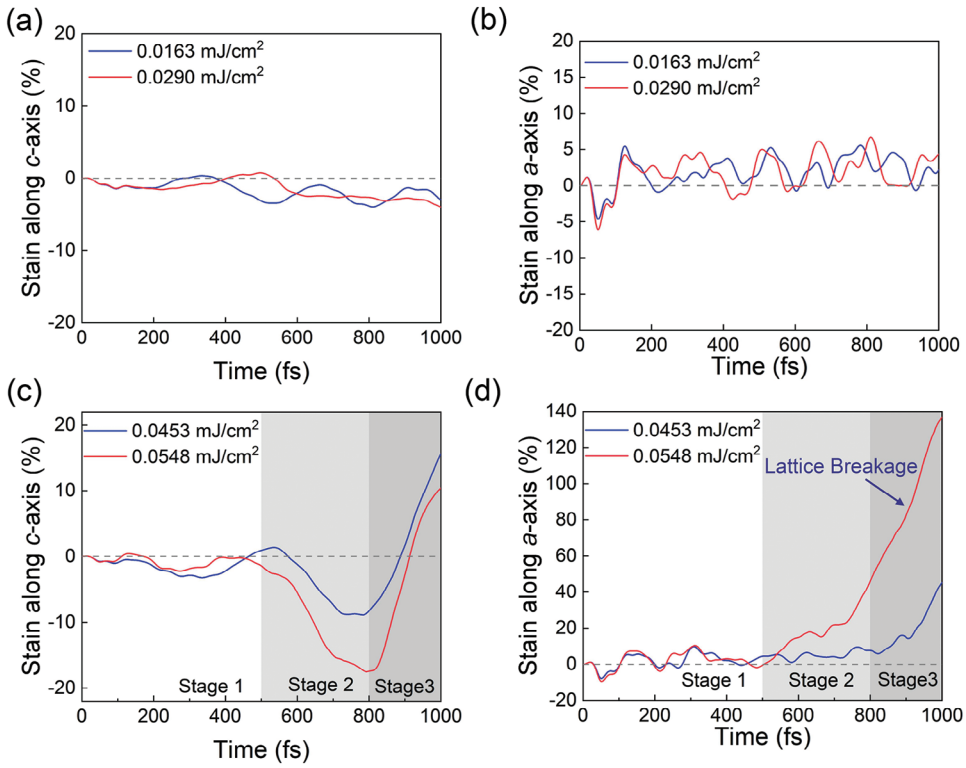

Figure 2. Time evolution of the lattice strains under the laser excitation. a,b) Under the low-energy light field, the strain of the lattice in the *c*-axis direction shows a slight contraction tendency (a) and the *a*-axis direction shows an unstable oscillation (b). c,d) Multistage lattice strains excited by higher laser energy. Along the *c*-axis, the lattice begins to compress at 500 fs, and reaches the maximum at 800 fs and begins to rebound and expand. The lattice keeps expanding in the *a*-axis direction until it breaks (stain rate more than 25%).

imately linear correlation. Hence, indirectly deducing the modulated lattice phase and its changes in $LiNbO_3$ stimulated by studying the material's refractive index is an acceptable approach.

2.3. Engineering Refractive Index Mutations in the Ultrafast Laser Direct Writing

In experiments, we utilize a femtosecond laser to locally modify the refractive index of $LiNbO_3$, enabling the production of waveguides and facilitating optical probing of refractive index changes. Unlike calculations that assume a uniformly excited lattice, the unirradiated region within the bulk material places limitations on the lattice strain within the irradiated region. Consequently, the final distribution of the refractive index is determined by a combination of factors such as laser processing parameters, lattice strain, stress, the elastic tensor, and temperature difference.[43] The laser-induced refractive index changes can be typically classified into two types: type I ($\Delta n > 0$) at low laser energy and type II modifications ($\Delta n < 0$) at high laser energy.[44–46] Traditionally,

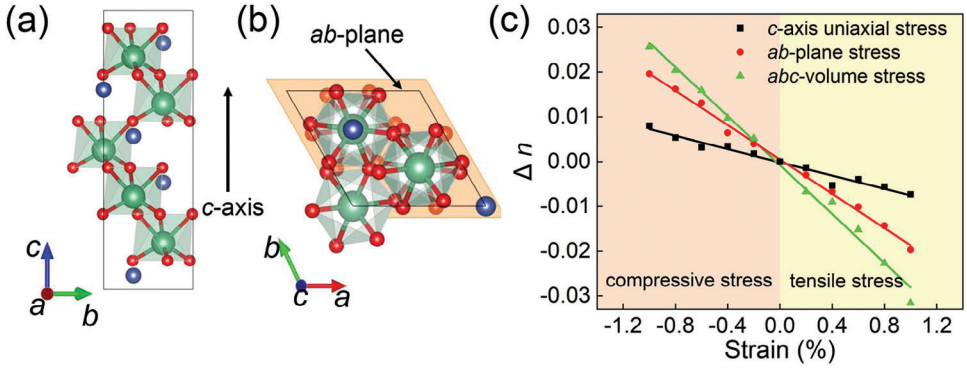

Figure 3. Influence of $LiNbO_3$ lattice strain on refractive index under compressive and tensile stresses with different crystalline phase orientations. a,b) Schematic of *c*-axis and *ab*-plane stress direction. c) Relationship between the lattice strain coefficient and refractive index of $LiNbO_3$.

when the incident laser energy is low, the rapid cooling of the focal edges induces internal stresses that lead to the formation of a denser structure, resulting in a slight local increase in refractive index (referred to as type I modification).[46] At the high energy regimes, multi-pulse incubation occurs, in which laser energy is rapidly deposited, generating a high-density plasma. This plasma triggers a Coulomb explosion that transports matter and energy out of the focus in the form of a shock wave, causing micro-explosions. As a consequence of this process, the refractive index at the focus decreases, known as type II modification.[47]

By adjusting the pulse energy (≈0.5–1.9 μJ), we observe a complete evolution from a gradual increase (type I) in refractive index to an abrupt decrease (type II) and even to micro-explosion (see Figure S4, Supporting Information, for more details). Our results are consistent with previous reports,[41] indicating that the transition from type I to type II manifests in the form of mutations. For type I modification characterized by an elevated refractive index, it is possible to reverse the damage through a heat treatment at 150 °C for 1 h, at which point the lattice recovers. When the incident laser energy surpasses 0.6 μJ (above the damage threshold), we observe the irrecoverable type II modifications in $LiNbO_3$.

The observed changes in refractive index, coinciding with the final strain state of the lattice as predicted by calculations, are indicative of a transition from type I to type II. However, to validate the accuracy of our model, it is imperative to visualize the multistage lattice evolution processes. Unfortunately, real-time probe detection techniques to verify the proposed mechanism of transient lattice volume contraction-expansion are not yet well-established. Therefore, we propose indirect evidence to support our claim by maintaining the transiently contracted state of the lattice near the strain threshold. In the case of ultrafast laser processing, it exhibits non-thermal properties, and the energy in the irradiation region demonstrates strong localization.[5] The tight focusing of the incident laser is a Gaussian distribution with an energy gradient (Figure S5 and Note S7, Supporting Information), which inevitably leads to small-scale non-uniform irradiation. Hence, we anticipate that as the laser energy approaches the mutation threshold, the central and sub-central regions irradiated by the laser will exhibit distinct types of lattice strains.

2.3.1. The Gradual Change of the Lattice from Contraction to Expansion

Experimentally, adjusting the focal depth results in better control of laser energy at the focus, enabling the successful observation of non-uniform refractive index modifications in both the irradiation center and sub-irradiation areas, as depicted in **Figure 4**a. The laser energy used is 0.5 μJ, and laser incident depth ranges from 208 to 200 μm. When the incident depth is 208 μm, the laser energy does not exceed the damage threshold of the $LiNbO_3$. Consequently, the lattice in the irradiated area contracts along the *c*-axis (type I modification), leading to an increase in refractive index (Figure 4 a1). By using transverse magnetic (TM) and transverse electric (TE) polarized lights for pumping (see Figure S6, Supporting Information), the waveguide mode can accurately represent the distribution of anisotropic refractive index and lattice strains in different axial directions, as demonstrated in Figure 4b,c. There is a significant difference in the mode-field distribution and propagation loss between the vertical and directions, implying that the refractive index changes variably along the different crystal axes (*c*- and *a*-axes). Among these, only the TM polarized light (*c*-axis direction) displays relatively stable output. This suggests an increase in the extraordinary refractive index (n_e) and a contraction of the lattice production along the *c*-axis direction. It is consistent with the calculation results in Figure 2a.

As illustrated in Figure 4a2, with a slight reduction in the depth of focus to ≈206.79 μm, the refractive index of the irradiation center area increases significantly, while the index of the sub-irradiation area changes slightly. We attribute this phenomenon to the energy gradient of the incident Gaussian light field. The incident energy in the irradiation center attains its mutation threshold, while the sub-irradiation area remains in type I modification. According to theoretical models, the lattice in the illuminated central region will experience rapid contraction followed by a rebound under the influence of a strong light field. Nonetheless, the sub-irradiated area has not yet reached this threshold and continues to display slight shrinkage stress. Once the lattice in the irradiation center area is induced to contract, it cannot expand because its rebound stress is lower than the extrusion stress from the surrounding lattice. Owing to the thermal and localized characteristics of ultrafast laser processing, the lattice cools swiftly, allowing us to effectively maintain the unusual contraction state of the lattice (Stage 2). As depicted in Figure 4a3–a5, with the depth of focus, decreasing (203.76–200.27 μm), the laser intensity at the central area is further enhanced, resulting in more pronounced rapid contraction and increased rebound stress. When the expansion stress exceeds the extrusion stress of the surrounding lattice, the lattice in the central region undergoes rapid expansion, eventually leading to the Coulomb explosion, corresponding to Stage 3 in Figure 2c. Therefore, we believe there is a reasonable consistency between the multi-stage dynamic processes in the calculation and the experimental results. Meanwhile, the waveguide modes (Figure 4 b4,b5) take on a doughnut-shaped form, further demonstrating the reduction of the central refractive index. This fine-tuning of energy offers a visualization of the transient dynamic process of multi-stage lattice contraction-expansion as the laser approaches the abrupt threshold, providing a valuable complement and proof to our model.

The micro-Raman scattering detection technique has been employed to analyze the phonon vibration mode and structural changes in the laser-induced lattice (Figure S7, Supporting Information). By exciting the specific phonon mode (Figure 1c), we have normalized the resonance peak of the active vibration mode (A_1-TO_4), as depicted in Figure 4d–f. It is evident from Figure 4 d1 that the Raman intensity at the lattice contraction has been reduced. Further, Figure 4 d2–d5 demonstrates that the more intense the lattice evolution, the lower the TO_4 phonon mode activity. In addition, Figure 4e illustrates the frequency shift of the Raman phonon mode, indicating a transition from compression to elongation of the oxygen octahedra in the irradiated central region. This observation is consistent with the observed increment or reduction of the refractive index. The assessment of material homogeneity and damage can be determined by measuring the broadening of the phonons emission. Figure 4 f1,f2 demonstrates minor changes in broadening, suggesting only slight deformation of the lattice structure. However, Figure 4 f3–f5 exhibits a significant increase in emission broadening, indicating a

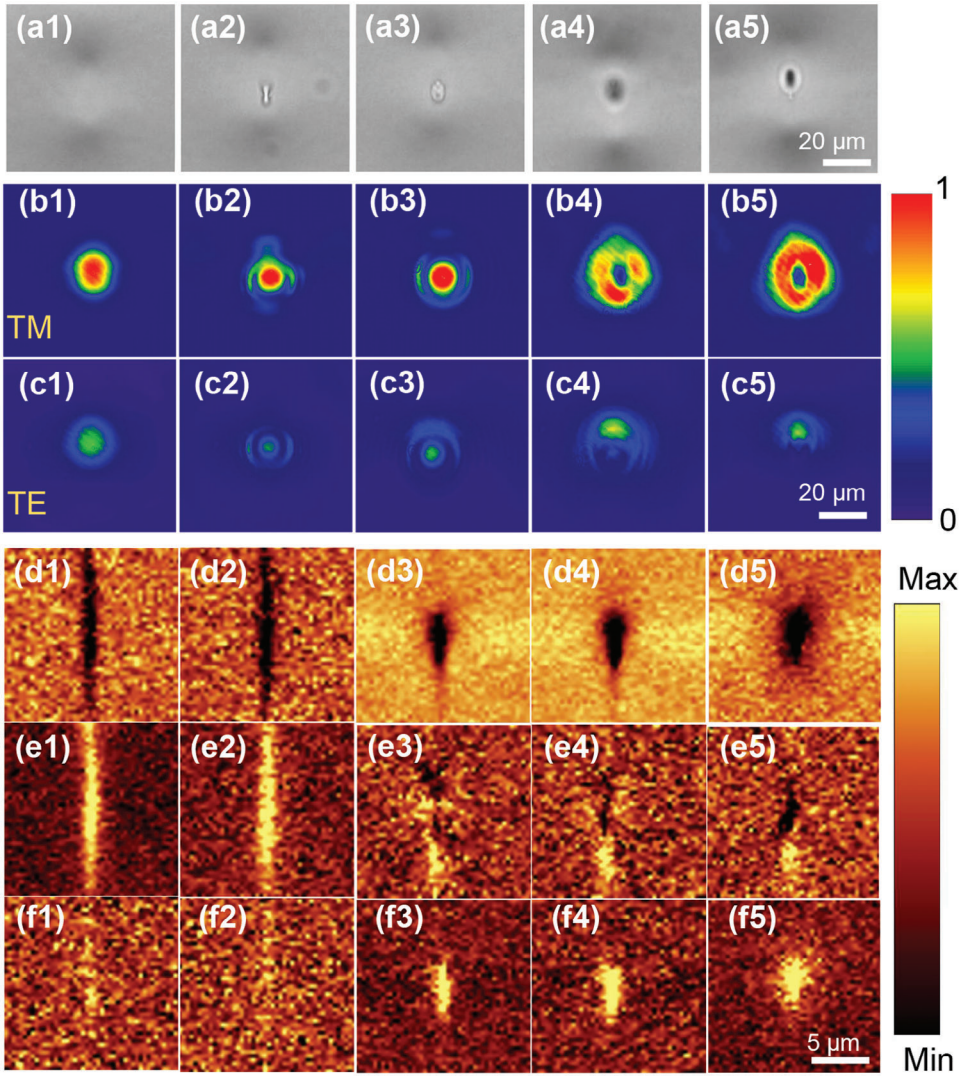

Figure 4. The gradual change of the lattice from contraction to expansion. The laser energy is fixed at 0.5 μJ, and the depth of focus is 208, 206.79, 203.76, 202.51, and 200.27 μm, respectively. a) Corresponding optical microscope images. b,c) Near-field mode profiles excited by TM and TE polarized light. d–f) The characteristic Raman peak of TO_4 is selected as the object of study, and the corresponding Raman intensity (d), frequency shift (e), and broadening of emission (f) are demonstrated.

decrease in material uniformity in the central region. These experimental findings align closely with the model, confirming the feasibility and effectiveness of utilizing rt-TDDFT for modeling complex crystalline materials.

2.3.2. Lattice Structure Changes in Ultra-Intense Light Fields

Moreover, as the energy levels exceed 0.6 μJ, the lattice experiences a rapid expansion, accompanied by stress from micro-explosions that compress the unirradiated regions, ultimately leading to an increased refractive index of the surrounding lattice. The lattice extrusion, illustrated in Figure S8a–c, Supporting Information (more details in Supporting Information), gradually extends from both sides of the irradiated area until it reaches the entire periphery. As the energy levels surpass a certain threshold (>1.7 μJ), a ring appears at a position further away from the irradiated area, which we attribute to the influence of a more powerful micro-explosion-induced shock wave (Figure S8d–f, Supporting Information). By combining theoretical calculations and experiments, we have comprehensively elucidated the process of laser-induced lattice motion and the resulting modulation of $LiNbO_3$. This research establishes the foundation for achieving precise control over nonlinear crystals and the realization of complex embedded optic chips.

3. Conclusions

In summary, this study provides new insights into the physical mechanisms and dynamic evolution of the interaction between ultrafast lasers and $LiNbO_3$, which is pivotal for precisely controlling the unique properties of this material. The rt-TDDFT

approach is used to simulate the dynamic processes of laser-induced lattice dynamics in $LiNbO_3$, which accurately characterizes the instantaneous evolution and displacive-type structural transitions of the $LiNbO_3$ lattice under diverse excitation levels and electron–phonon coupling. Besides, we have achieved two opposite modifications of the refractive index in $LiNbO_3$ and provided compelling evidence for this theory through comprehensive visualization of the refractive index and lattice evolution. This work serves as a cornerstone for further research on multistage lattice strains and lattice dynamics in laser-induced crystalline materials. Moreover, our study contributes to the advancement of advanced photonic devices and holds immense potential for application in the fields of optical communications and information processing.

Supporting Information

Supporting Information is available from the Wiley Online Library or from the author.

Acknowledgements

B.W. and Q.Y. contributed equally to this work. This work was supported by the National Natural Science Foundation of China (Grant Nos. 12174222, 12147130), the Natural Science Foundation of Shandong Province (Grant No. ZR2021ZD02), the National Key Research and Development Program of China (Grant No. 2021YFA1400201), and the China Postdoctoral Science Foundation (Grant No. 2021M693371).

Conflict of Interest

The authors declare no conflict of interest.

Data Availability Statement

The data that support the findings of this study are available from the corresponding author upon reasonable request.

Keywords

femtosecond laser direct writing, light-matter interactions, lithium niobate, real-time dynamic evolution calculation

Received: August 30, 2023
Revised: October 24, 2023
Published online:

[1] H. Lakhotia, H. Y. Kim, M. Zhan, S. Hu, S. Meng, E. Goulielmakis, *Nature* **2020**, *583*, 55.
[2] J. Bang, Y. Y. Sun, X. Q. Liu, F. Gao, S. B. Zhang, *Phys. Rev. Lett.* **2016**, *117*, 126402.
[3] S. Duan, Y. Cheng, W. Xia, Y. Yang, C. Xu, F. Qi, C. Huang, T. Tang, Y. Guo, W. Luo, D. Qian, D. Xiang, J. Zhang, W. Zhang, *Nature* **2021**, *595*, 239.
[4] A. Ródenas, M. Gu, G. Corrielli, P. Paiè, S. John, A. K. Kar, R. Osellame, *Nat. Photonics* **2018**, *13*, 105.
[5] S. K. Sundaram, E. Mazur, *Nat. Mater.* **2002**, *1*, 217.
[6] P. Lorazo, L. J. Lewis, M. Meunier, *Phys. Rev. Lett.* **2003**, *91*, 225502.
[7] Y. Bellouard, A. Champion, B. McMillen, S. Mukherjee, R. R. Thomson, C. Pépin, P. Gillet, Y. Cheng, *Optica* **2016**, *3*, 1285.
[8] P. Vlugter, Y. Bellouard, *Phys. Rev. Mater.* **2022**, *6*, 033602.
[9] L. Arizmendi, *Phys. Status Solidi A* **2004**, *201*, 253.
[10] M. Zhang, C. Wang, P. Kharel, D. Zhu, M. Lončar, *Optica* **2021**, *8*, 652.
[11] Y. Li, Q. Wu, M. Yang, Q. Li, Z. Chen, C. Zhang, J. Sun, J. Yao, J. Xu, *Appl. Surf. Sci.* **2019**, *478*, 779.
[12] X. Porte, N. U. Dinc, J. Moughames, G. Panusa, C. Juliano, M. Kadic, C. Moser, D. Brunner, D. Psaltis, *Optica* **2021**, *8*, 1281.
[13] J. Lin, N. Yao, Z. Hao, J. Zhang, W. Mao, M. Wang, W. Chu, R. Wu, Z. Fang, L. Qiao, W. Fang, F. Bo, Y. Cheng, *Phys. Rev. Lett.* **2019**, *122*, 173903.
[14] M. Henstridge, M. Först, E. Rowe, M. Fechner, A. Cavalleri, *Nat. Phys.* **2022**, *18*, 457.
[15] X. Xu, T. Wang, P. Chen, C. Zhou, J. Ma, D. Wei, H. Wang, B. Niu, X. Fang, D. Wu, S. Zhu, M. Gu, M. Xiao, Y. Zhang, *Nature* **2022**, *609*, 496.
[16] D. Wei, C. Wang, X. Xu, H. Wang, Y. Hu, P. Chen, J. Li, Y. Zhu, C. Xin, X. Hu, Y. Zhang, D. Wu, J. Chu, S. Zhu, M. Xiao, *Nat. Commun.* **2019**, *10*, 4193.
[17] S. Liu, K. Switkowski, C. Xu, J. Tian, B. Wang, P. Lu, W. Krolikowski, Y. Sheng, *Nat. Commun.* **2019**, *10*, 3208.
[18] J. Burghoff, H. Hartung, S. Nolte, A. Tünnermann, *Appl. Phys. A* **2006**, *86*, 165.
[19] J. Burghoff, S. Nolte, A. Tünnermann, *Appl. Phys. A* **2007**, *89*, 127.
[20] S. Kudryashov, A. Rupasov, M. Kosobokov, A. Akhmatkhanov, G. Krasin, P. Danilov, B. Lisjikh, A. Turygin, E. Greshnyakov, M. Kovalev, A. Efimov, V. Shur, *Nanomaterials* **2022**, *12*, 4147.
[21] V. Caciuc, A. V. Postnikov, G. Borstel, *Phys. Rev. B* **2000**, *61*, 8806.
[22] E. Bagli, V. Guidi, A. Mazzolari, L. Bandiera, G. Germogli, A. I. Sytov, D. De Salvador, A. Argiolas, M. Bazzan, A. Carnera, A. Berra, D. Bolognini, D. Lietti, M. Prest, E. Vallazza, *Phys. Rev. Lett.* **2015**, *115*, 015503.
[23] K. R. Ferguson, M. Bucher, T. Gorkhover, S. Boutet, H. Fukuzawa, J. E. Koglin, Y. Kumagai, A. Lutman, A. Marinelli, M. Messerschmidt, K. Nagaya, J. Turner, K. Ueda, G. J. Williams, P. H. Bucksbaum, C. Bostedt, *Sci. Adv.* **2016**, *2*, e1500837.
[24] S. Gerber, S.-L. Yang, D. Zhu, H. Soifer, J. A. Sobota, S. Rebec, J. J. Lee, T. Jia, B. Moritz, C. Jia, A. Gauthier, Y. Li, D. Leuenberger, Y. Zhang, L. Chaix, W. Li, H. Jang, J.-S. Lee, M. Yi, G. L. Dakovski, S. Song, J. M. Glownia, S. Nelson, K. W. Kim, Y.-D. Chuang, Z. Hussain, R. G. Moore, T. P. Devereaux, W.-S. Lee, P. S. Kirchmann, et al., *Science* **2017**, *357*, 71.
[25] I. Inoue, Y. Deguchi, B. Ziaja, T. Osaka, M. M. Abdullah, Z. Jurek, N. Medvedev, V. Tkachenko, Y. Inubushi, H. Kasai, K. Tamasaku, T. Hara, E. Nishibori, M. Yabashi, *Phys. Rev. Lett.* **2021**, *126*, 117403.
[26] P. Fons, P. Rodenbach, K. V. Mitrofanov, A. V. Kolobov, J. Tominaga, R. Shayduk, A. Giussani, R. Calarco, M. Hanke, H. Riechert, R. E. Simpson, M. Hase, *Phys. Rev. B* **2014**, *90*, 094305.
[27] L. Waldecker, T. A. Miller, M. Rude, R. Bertoni, J. Osmond, V. Pruneri, R. E. Simpson, R. Ernstorfer, S. Wall, *Nat. Mater.* **2015**, *14*, 991.
[28] R. Li, K. Sundqvist, J. Chen, H. E. Elsayed-Ali, J. Zhang, P. M. Rentzepis, *Struct. Dyn.* **2018**, *5*, 044501.
[29] H. Tanimura, S. Watanabe, T. Ichitsubo, *Adv. Funct. Mater.* **2020**, *30*, 2002821.
[30] N. V. Sidorov, N. A. Teplyakova, M. N. Palatnikov, L. A. Aleshina, O. V. Sidorova, A. V. Kadetova, *J. Solid State Chem.* **2020**, *282*, 121109.
[31] R. Mankowsky, A. von Hoegen, M. Forst, A. Cavalleri, *Phys. Rev. Lett.* **2017**, *118*, 197601.
[32] H. W. Lin, G. Mead, G. A. Blake, *Phys. Rev. Lett.* **2022**, *129*, 207401.
[33] K. Parlinski, Z. Q. Li, Y. Kawazoe, *Phys. Rev. B* **2000**, *61*, 272.

[34] X.-P. Wang, X.-B. Li, N.-K. Chen, J. Bang, R. Nelson, C. Ertural, R. Dronskowski, H.-B. Sun, S. Zhang, *npj Comput. Mater.* **2020**, *6*, 31.
[35] N. K. Chen, X. B. Li, J. Bang, X. P. Wang, D. Han, D. West, S. Zhang, H. B. Sun, *Phys. Rev. Lett.* **2018**, *120*, 185701.
[36] M. Först, C. Manzoni, S. Kaiser, Y. Tomioka, Y. Tokura, R. Merlin, A. Cavalleri, *Nat. Phys.* **2011**, *7*, 854.
[37] B. A. Nogueira, M. Rérat, R. Fausto, C. Castiglioni, R. Dovesi, *J. Raman Spectrosc.* **2022**, *53*, 1904.
[38] S. Meng, E. Kaxiras, *J. Chem. Phys.* **2008**, *129*, 054110.
[39] W. Liu, J. Luo, S. Li, L. Wang, *npj Comput. Mater.* **2021**, *7*, 117.
[40] M. X. Guan, X. B. Liu, D. Q. Chen, X. Y. Li, Y. P. Qi, Q. Yang, P. W. You, S. Meng, *Phys. Rev. Lett.* **2022**, *128*, 015702.
[41] B. Zhang, L. Wang, F. Chen, *Laser Photonics Rev.* **2020**, *14*, 1900407.
[42] J. Imbrock, L. Wesemann, S. Kroesen, M. Ayoub, C. Denz, *Optica* **2020**, *7*, 28.
[43] H. D. Nguyen, A. Rodenas, J. R. Vazquez de Aldana, J. Martinez, F. Chen, M. Aguilo, M. C. Pujol, F. Diaz, *Opt. Express* **2016**, *24*, 7777.
[44] D. Tan, Z. Wang, B. Xu, J. Qiu, *Adv. Photonics* **2021**, *3*, 024002.
[45] F. Chen, J. R. V. de Aldana, *Laser Photonics Rev.* **2014**, *8*, 251.
[46] L. Li, W. Kong, F. Chen, *Adv. Photonics* **2022**, *4*, 024002.
[47] D. Tan, B. Zhang, J. Qiu, *Laser Photonics Rev.* **2021**, *15*, 2000455.